ENVIRONMENTAL ENGINEERING SCIENCE
Volume 32, Number 2, 2015

DOI: 10.1089/ees.2014.0335

Fate and Transport of Molybdenum Disulfide Nanomaterials in Sand Columns

Jacob D. Lanphere,[1] Corey J. Luth,[1] Linda M. Guiney,[2] Nikhita D. Mansukhani,[2] Mark C. Hersam,[2] and Sharon L. Walker[1,*,**]

[1]*Department of Chemical and Environmental Engineering, University of California, Riverside, California.*
[2]*Department of Material Science and Engineering, Chemistry, and Medicine, Northwestern University, Evanston, Illinois.*

Received: July 9, 2014 *Accepted in revised form: September 26, 2014*

Abstract

Research and development of two-dimensional transition metal dichalcogenides (TMDC) (e.g., molybdenum disulfide [MoS_2]) in electronic, optical, and catalytic applications has been growing rapidly. However, there is little known regarding the behavior of these particles once released into aquatic environments. Therefore, an in-depth study regarding the fate and transport of two popular types of MoS_2 nanomaterials, lithiated (MoS_2-Li) and Pluronic PF-87 dispersed (MoS_2-PL), was conducted in saturated porous media (quartz sand) to identify which form would be least mobile in aquatic environments. The electrokinetic properties and hydrodynamic diameters of MoS_2 as a function of ionic strength and pH were determined using a zeta potential analyzer and dynamic light scattering techniques. Results suggest that the stability is significantly decreased beginning at 10 and 31.6 mM KCl, for MoS_2-PL and MoS_2-Li, respectively. Transport study results from breakthrough curves, column dissections, and release experiments suggest that MoS_2-PL exhibits a greater affinity to be irreversibly bound to quartz surfaces as compared with the MoS_2-Li at a similar ionic strength. Derjaguin–Landau–Verwey–Overbeek theory was used to help explain the unique interactions between the MoS_2-PL and MoS_2-Li surfaces between particles and with the quartz collectors. Overall, the results suggest that the fate and transport of MoS_2 is dependent on the type of MoS_2 that enters the environment, where MoS_2-PL will be least mobile and more likely be deposited in porous media from pluronic–quartz interactions, whereas MoS_2-Li will travel greater distances and have a greater tendency to be remobilized in sand columns.

Key words: effects of pH and ionic strength; molybdenum disulfide (MoS_2); nanomaterials; pluronic coating; transport in packed bed column; stability; straining

Introduction

TWO-DIMENSIONAL NANOMATERIALS have gained a significant amount of attention recently (Cooper *et al.*, 2013). The most common two-dimensional material has traditionally been graphene (Lotya *et al.*, 2009) or its oxidized derivative graphene oxide (Compton and Nguyen, 2010). However, research and development of molybdenum disulfide (MoS_2), a two-dimensional transition metal dichalcogenide (TMDC) has been increasing over the last few years (Gong *et al.*, 2013) and is beginning to rival the popularity of graphene for monolayer materials (Liu *et al.*, 2014). In 2012, an editorial in the journal *Nature* noted that ''Graphene is Not Alone'' and that TMDCs are gaining a tremendous amount of attention with tungsten disulfide (WS_2) and MoS_2 leading the way for future optical and electronic applications (Wang *et al.*, 2012b). MoS_2 is a layered TMDC, which includes two planes of sulfur (S) atoms with a single plane of molybdenum (Mo) atom in the center of the structure with the Mo and S atoms being bound together by covalent bonds (Silbernagel, 1975).

The rise in popularity with MoS_2 is due to its many novel electrical and optical properties (Najmaei *et al.*, 2014), including a tunable band gap (Lopez-Sanchez *et al.*, 2013), exceptional photo-response (Lopez-Sanchez *et al.*, 2013), and high charge carrier mobility (Wang *et al.*, 2012a). MoS_2 is also a direct band gap semiconductor (Zhou *et al.*, 2013), which could make it an ideal material for transistors or optoelectronics devices (Mak *et al.*, 2010). Other applications for MoS_2 include lithium ion batteries (Stephenson *et al.*, 2014), electrochemical charge storage (Winchester *et al.*,

*Member of AEESP.
***Corresponding author:* Department of Chemical and Environmental Engineering, University of California, Riverside, CA 92521. *Phone:* (951) 827-6094; *Fax:* (951) 827-5696; *E-mail:* swalker@engr.ucr.edu

2014), lubricants (Khare and Burris, 2014), and ultra-fast photonics (Zhang *et al.*, 2014). With the widespread research and development of engineered nanomaterials, the implementation of MoS_2 nanomaterials has also gained a tremendous amount of interest for use in nanotechnological applications (e.g., catalysts, and nanotubes) (Lauritsen *et al.*, 2007). Whereas the production and development of MoS_2 NPs has a tremendous technological potential, there is a lack of knowledge and research regarding its behavior if released into the environment. To the authors' knowledge, there are no reports that investigate the fate or transport of MoS_2 in aquatic environments.

In the past, it has been reported that other two-dimensional nanomaterials (e.g., graphene oxide) can exhibit toxic effects on living organisms (e.g., increased mitochondrial respiration in mice) (Duch *et al.*, 2011). Currently there is little information regarding the potential toxicity of MoS_2 nanomaterials. In 2011, Wu *et al.* (2011) reported that inorganic fullerene-like MoS_2 nanomaterials prepared using pulsed laser ablation were biocompatible and provided a green method to synthesize nanomaterials. However, it has been reported in the past that elevated levels of molybdenum (Mo) in ruminate intake can result in a physiological copper (Cu) deficiency, which may have negative consequences (Ward, 1978).

In 2013, Keller *et al.* (2013) reported that it is highly likely that some portion of engineered nanomaterials that reach a landfill will make their way into the surrounding environment. In 2014, Conway *et al.* (2014) reported that phytoplankton sorbed engineered nanomaterials (CeO_2) in less than 1 h and had negative impacts on marine mussels in seawater environments. This suggests that if the careful implementation of nanomaterials is not employed, then their accidental release into the environment may occur and have long-lasting effects on aquatic life. Therefore, it is crucial that the science community and policy makers have a comprehensive set of research data to help predict the fate and transport of MoS_2 nanomaterials once introduced into aquatic environments.

This study is set forth to bridge the gap of knowledge regarding the influence that environmentally relevant parameters (e.g., ionic strength and pH) will have on the fate, transport, and aggregate morphology of the two forms of MoS_2 nanomaterials: Lithiated (MoS_2-Li) and Pluronic (MoS_2-PL). MoS_2-Li is exfoliated through a lithiation process, during which lithium ions intercalate into the layered bulk material and enable the exfoliation of the material using gentle sonication. A dialysis step following the exfoliation removes the lithium ions as well as any residual organics, leaving only trace amounts of lithium present on the surface of the nanomaterial. The exfoliation process produces two-dimensional flakes of MoS_2 that are overall negatively charged and thus remain dispersed in aqueous environments without the addition of surfactants. The MoS_2-Li was chosen since this represents the most scalable and controllable synthesis method for monolayer MoS_2 that will likely be used in the future, therefore, representing one of the most abundant forms of two-dimensional MoS_2 that would be found in the environment. On the other hand, MoS_2-PL is exfoliated by ultrasonication with the aid of a biocompatible triblock copolymer, commercially available as Pluronic, which acts as a surfactant and stabilizes the MoS_2 flakes in aqueous solution. The Pluronic triblock copolymer is a linear molecule containing a central hydrophobic chain of polypropylene oxide (PPO) functional groups and is bordered by two hydrophilic chains of polyethylene oxide (PEO) of equal length (Seo *et al.*, 2011). It is predicted that for industrial applications, a stable and monodisperse suspension of MoS_2 will be required and, therefore, surfactants will play an increasing role in MoS_2 nanotechnology development (Vaisman *et al.*, 2006). Recent studies have also reported using Pluronic surfactants to stabilize carbon nanotubes (Vaisman *et al.*, 2006), and other two-dimensional nanomaterials such as graphene (Seo *et al.*, 2011). Therefore, in this study, Pluronic PF-87 was chosen as a representative surfactant to produce an additional form of dispersed MoS_2 to investigate its behavior in aquatic environments.

This study is the first to report the effects of two important environmentally relevant parameters (i.e., ionic strength and pH) on MoS_2 nanomaterials stability and transport in a packed bed column and provides critical information regarding how interactions between quartz surfaces influence the transport of MoS_2-PL and MoS_2-Li. This report also helps to answer the question of whether traditional colloid filtration theory can apply to the planar TMDCs. The results from this report help to explain the behavior of MoS_2 in engineered or natural systems where they may settle or deposit on sediments in the subsurface and sheds light on the chemical and physical mechanisms responsible for this behavior.

Experimental Protocols

Molybdenum disulfide

The MoS_2 nanomaterials used in this study were synthesized by the following process. To synthesize the lithiated MoS_2 (MoS_2-Li), lithium intercalation was achieved by combining MoS_2 powder with butyllithium in a low vapor and oxygen environment for 2 days while stirring. The MoS_2-Li was retrieved from the solution by filtration and immersed in deionized water. To avoid deintercalation, the exfoliation was carried out immediately using a bath sonicator. A centrifugation step was performed to remove unexfoliated material. The resulting supernatant was dialyzed for 7 days in a bath of deionized water to remove any excess lithium and hexane. To synthesize the pluronic MoS_2 (MoS_2-PL), MoS_2 powder was exfoliated by ultrasonication in a solution of 2% w/v Pluronic F87 in deionized water.

Following ultrasonication, the slurry was centrifuged to remove any unexfoliated material and aggregates. Only the top 80% of the supernatant was retained. The lithiated MoS_2 (MoS_2-Li) used in this study had a mean square root surface area of $(187.5 \pm 126.9\,\text{nm})^2$, a mean height of 3.9 ± 0.6 nm, and a mean perimeter of 689.1 ± 433.0 nm. Whereas the pluronic MoS_2 (MoS_2-PL) used in this study had a mean square root surface area of $(27.6 \pm 15.6\,\text{nm})^2$, an average height of 5.2 ± 1.1 nm, and an average perimeter of 100.8 ± 57.3 nm. The MoS_2-PL and MoS_2-Li were previously dispersed in deionized (DI) water at stock concentrations of 0.125 and 0.038 mg/mL, respectively. To create 10 mg/L MoS_2 dilutions at each ionic strength (IS) used in this study (0.1–100 mM KCl), MoS_2 nanomaterials were introduced to the electrolyte and either vortexed (Fisher Scientific, Mini Vortexer) or lightly shaken for ≥ 5 s. Potassium chloride (KCl) was used as the background electrolyte (ACS Research Grade, Fisher Scientific, Pittsburgh, PA) in all experiments. The unadjusted pH of the MoS_2-Li and MoS_2-PL stock suspensions were 3.9 ± 0.1 and 5.3 ± 0.1, respectively. Potassium hydroxide

(KOH) and hydrochloric acid (HCl) were used to adjust the pH of the MoS_2 suspensions. All MoS_2 suspensions were created using DI water (nanopure water at $>18.2\,M\Omega$ cm at 25°C).

General characterization of nanomaterials and porous media

Electrokinetic properties and hydrodynamic diameter of MoS_2. The influence of pH and ionic strength (IS) on the MoS_2-PL and MoS_2-Li was determined by measuring the effective hydrodynamic diameter and electrophoretic mobility (EPM) across an environmentally relevant pH range of 4–10 and an IS range of 0.1–100 mM KCl, respectively. Dynamic light scattering (Brookhaven model BI-9000, Holtsville, NY) measurements taken at a wavelength of 661 nm and a scattering angle of 90° were used to determine the effective hydrodynamic diameter of the MoS_2 suspensions. The EPM was measured using a ZetaPALS analyzer (Brookhaven Instruments, Holtsville, NY). Triplicate measurements were taken at room temperature ($23°C \pm 1°C$) for all of these electrokinetic and size measurements.

Elektrokinetic characterization of quartz. Additional characterization of the quartz sand collectors was performed to help explain any potential interactions between the MoS_2 particles and the quartz surfaces during transport in the packed bed column and was used in the application of DLVO theory (Tables 2 and 3). The streaming potential of the quartz sand (used as the porous media in the column experiments) was measured using a streaming potential analyzer (surPASS, Anton Paar, Graz, Austria). Triplicate measurements were taken in deionized water at pH 5 and across the same range of ionic strength (1–31.6 mM KCl) conditions used in the transport experiments.

Scanning electron microscope images of MoS_2 and quartz. Scanning Electron Microscopy (SEM) images were taken of the dried aggregated MoS_2 nanoparticles on quartz slides. MoS_2 samples were prepared by adding $\sim 15\,\mu L$ of stock MoS_2-PL and MoS_2-Li at an unadjusted pH in deionized water to quartz slides and were allowed to dry overnight before taking SEM images. The SEM images of the quartz sand used as porous media in the column experiments were also taken. Quartz samples were prepared by adding a small amount ~ 30 sand grains in deionized water to a quartz slide and left to dry overnight.

Packed bed column transport experiments

The effect of ionic strength (1–31.6 mM KCl) on the transport of MoS_2-Li and MoS_2-PL in saturated porous media was conducted using a packed bed column at pH 5. Transport experiments were conducted using an inverted borosilicate glass column (Omnifit, Boonton, NJ) with an inner diameter of 1.5 cm and a packing depth of 5 cm. Details regarding the packed bed column transport methods, conditions, and sand cleaning procedures can be found elsewhere (Lanphere *et al.*, 2013). Briefly, quartz sand was sieved to obtain an average diameter (d_{50}) of $275\,\mu m$ and purified before being wet packed at a porosity of 0.47 ± 0.01 in the column before transport experiments. MoS_2 suspensions were injected into the column at a flow rate of 2 mL/min to represent similar flow conditions found in the engineered or natural systems (Hemond, 2009) using peristaltic pumps and the effluent was collected every minute using a fraction collector (CF 1 Fraction Collector, Spectrum Chromatography, Houston, TX). The effluent was used to determine the concentration at each time interval using a spectrophotometer (DU 800 Beckman Coulter, Fullerton, CA) to correlate the absorbance with concentration. Calibration curves for the MoS_2-Li and MoS_2-PL were created by measuring the absorbance as a function of MoS_2 concentration and an R^2 value of 0.999 was obtained for both types of MoS_2.

Release experiments were also conducted following select transport experiment at each IS for MoS_2-PL and MoS_2-Li to investigate the release of particles as a function of the decrease in IS. To facilitate the release experiments, an additional 12 pore volumes (PV) of DI water was injected into the column after the background absorbance dropped to ~ 0 and the effluent was collected and the absorbance measured as mentioned earlier.

Column dissection

To evaluate the distribution by which MoS_2 was retained in the column, select columns were dissected following a transport experiment. Deposition profiles of MoS_2 at each centimeter in the column were developed from the column dissections to interpret the distribution of MoS_2 following an experiment at each ionic strength. The procedure for the column dissection can be found elsewhere (Lanphere *et al.*, 2013) and was based upon a previously developed protocol (Tufenkji and Elimelech, 2004). Briefly, once the experiments were completed, the bottom fitting of the column was removed and the background electrolyte was injected into the column. Next, the sand slowly flowed out of the column by gravity and approximately one centimeter portions of the sand were collected in centrifuge tubes as they came out of the column. The collected samples–comprising of quartz, KCl, and retained MoS_2 particles–were rinsed with 25 mL of DI water and vortexed for 30 s. The supernatant from this step was decanted into a centrifuge tube and saved for further analysis. This step was repeated twice to achieve a total volume (50 mL) of reversibly bound MoS_2. These MoS_2-containing supernatant suspensions were then taken to a spectrophotometer to measure the absorbance of the MoS_2-PL and MoS_2-Li suspensions obtained for each centimeter at wavelengths of 258 and 247 nm, respectively. The absorbance values for the supernatant collected at each centimeter were then correlated with MoS_2-PL and MoS_2-Li concentrations using the same calibration curves mentioned previously. The remaining sand at each centimeter from the dissected column was then dried and the mass was recorded. Results were then plotted as the mass of nanoparticles retained in each centimeter of sand [(mass of MoS_2 retained/mass of MoS_2 injected)/mass of quartz sand] dissected as a function of the depth of the column. These retention profiles were then developed to further understand the deposition behavior of MoS_2 throughout the column as a function of ionic strength.

Results and Discussion

Effects of pH and ionic strength on MoS_2 stability

To investigate the behavior of two leading MoS_2 nanomaterials to identify which one is least mobile in the

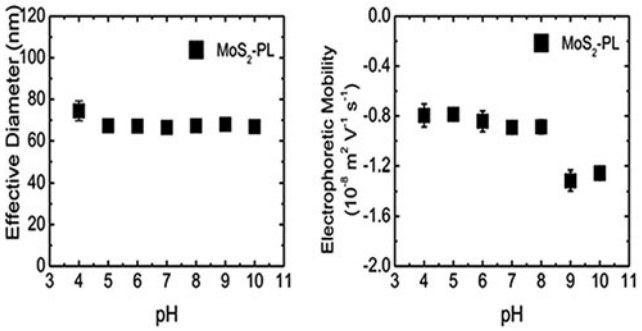

FIG. 1. MoS_2-PL evaluated as a function of pH for effective hydrodynamic diameter and electrophoretic mobility. MoS_2-PL concentration was maintained at 10 mg/L and 10 mM KCl. Error bars indicate one standard deviation of triplicate measurements.

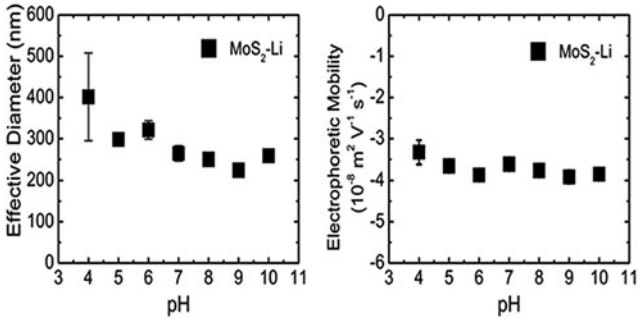

FIG. 3. MoS_2-Li evaluated as a function of pH for effective hydrodynamic diameter and electrophoretic mobility. MoS_2-Li concentration was maintained at 10 mg/L and 10 mM KCl. Error bars indicate one standard deviation of triplicate measurements.

environment, MoS_2-PL and MoS_2-Li were extensively characterized. It has been reported in the past (Elimelech and Omelia, 1990; Wiesner and Lecoanet, 2004; Chowdhury *et al.*, 2013) that nanoparticle size (Chen and Elimelech, 2006), and surface charge (Keller *et al.*, 2010b) characterization can provide critical insights into predicting the ultimate fate of these materials in the environment. Therefore, a comprehensive study was performed to investigate the effects of solution chemistry on MoS_2-Li and MoS_2-PL across an environmentally relevant range of aquatic chemistries and the results are shown in Figures 1–4. The pH range studied was 4–10, and the IS spectrum was 0.1–100 mM KCl. This wide range of solution chemistry covers not only environmental conditions for most natural water (e.g., lakes, and streams), (Hemond, 2009; Crittenden *et al.*, 2012), but extreme conditions as well (i.e., pH 9–10 and 31.6–100 mM KCl) (Hemond, 2009). The influence of pH on the diameter and EPM varied between the two types of MoS_2 tested as a function of their type. While it was expected that the size and surface charge of MoS_2-PL would not significantly change across the environmental pH range (5–9) tested due to the surfactant PF-87 coating present, it was not known what the behavior would be at the lower and upper pH values (4, 10). In addition, it was anticipated that MoS_2-Li would not be sensitive to pH (from 4 to 10) with respect to its diameter size and EPM as has been reported previously for other two-dimensional nanomaterials (e.g., graphene oxide) (Chowdhury *et al.*, 2013). Overall this hypothesis was correct and there was little effect on the effective diameter and EPM of MoS_2 as a function of pH within environmentally relevant parameters (pH 5–9). It was only when the pH was near or outside of this range when a significant difference in stability for MoS_2-Li and MoS_2-PL was observed (Figs. 1 and 3).

The effective diameter for MoS_2-Li (as measured by DLS) was much more sensitive to the change in pH than anticipated. Specifically, at pH 4, the effective diameter (401 ± 106 nm) for MoS_2-Li was $\sim 25\%$ larger than the effective diameter (298 ± 12 nm) at pH 5 as seen in Figure 3. However, there was no significant effect ($p > 0.05$) on the MoS_2-Li EPM across the range of pH (4–10) tested (Fig. 3). Similar results have been reported for other planar nanomaterials (e.g., graphene oxide) (Chowdhury *et al.*, 2013; Lanphere *et al.*, 2013) where no significant effect on EPM or diameter was observed from pH 5–9. However, in recent studies, the zeta potential of spherical nanoparticles [ZnO, (Mohd Omar *et al.*, 2014), Ag (Yin *et al.*, 2014), and TiO_2 (Wang *et al.*, 2014)] were shown to be sensitive to changes in pH across an environmentally relevant range (5–9). For the MoS_2-PL, the opposite trend occurred when compared with the MoS_2-Li with regard to the influence on diameter and EPM. Specifically, there was no significant effect ($p > 0.05$) in the diameter from pH 4–10, however, the EPM did significantly increase from -0.9 ± 0.1 to -1.4 ± 0.1 (10^{-8} $m^2/[V \cdot s]$) at pH 8 and 9, respectively. These results suggests that the MoS_2-PL will be the most stable across an environmental pH range (5–9) in natural

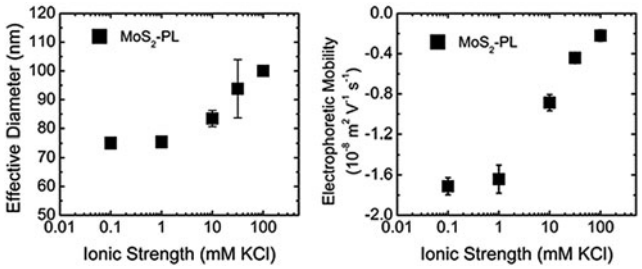

FIG. 2. MoS_2-PL evaluated as a function of ionic strength for effective hydrodynamic diameter and electrophoretic mobility. MoS_2-PL concentration was maintained at 10 mg/L and at an adjusted pH 5. Error bars indicate one standard deviation of triplicate measurements.

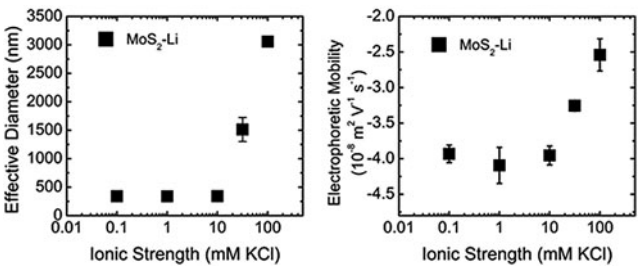

FIG. 4. MoS_2-Li evaluated as a function of ionic strength for effective hydrodynamic diameter and electrophoretic mobility. MoS_2-Li concentration was maintained at 10 mg/L and at an adjusted pH 5. Error bars indicate one standard deviation of triplicate measurements.

waters and will not likely be removed during transport in sediment beds since the effective diameter will remain small as a result of the PF-87 coating. However, for the MoS_2-Li, the sensitivity to low pH (<5) with respect to the increase in effective diameter, may result in the MoS_2-Li being settled down or sediments removed.

It was anticipated that the increase in IS would decrease the electrostatic double layer repulsion between the MoS_2 NPs and, therefore, result in the increased aggregation as has been reported in other nanoparticle studies (Keller *et al.*, 2010a; Petosa *et al.*, 2010, 2012; Chowdhury *et al.*, 2011) with TiO_2, ZnO, and CeO_2. However, it was unknown how these effects of IS would vary amongst the two types of MoS_2 characterized in this study or at what IS would cause a significant change.

In general, the MoS_2-PL and MoS_2-Li became less stable (as observed by an increase in effective diameter and a decrease in EPM) as a function of IS (Figs. 2 and 4, respectively). The average effective hydrodynamic diameters of the MoS_2-Li and MoS_2-PL were measured in DI water and were 345 ± 4 and 81 ± 1 nm, respectively. A significant effect ($p < 0.05$) of IS on the effective diameter of MoS_2-Li did not occur until 31.6 mM KCl was achieved when the diameter increased from 340 ± 13 to 1795 ± 413 nm, respectively. Furthermore, the MoS_2-Li effective diameter increased almost by an order of magnitude from 340 ± 13 nm to 3057 ± 402 nm, across the range of 0.1–100 mM KCl.

This increase in MoS_2-Li aggregate diameter as a function of IS is likely a result of the decrease in electric double layer repulsion at higher IS and is in agreement with previous studies performed with carbon nanotubes (Chowdhury *et al.*, 2012b). However, the effective diameter of the MoS_2-PL remained fairly constant (81 ± 7 nm) across the IS range tested, and only increased by $\sim 17\%$ from 0.10 to 100 mM KCl. This was expected as a result of the pluronic surfactant coating on the MoS_2, which limited its aggregation as a function of IS. Similar results have been reported for other engineered nanomaterials [e.g., fullerenes (Xie *et al.*, 2008), and TiO_2 (Chowdhury *et al.*, 2012a)] coated with natural organic matter where an increase in particle stability (as observed by a reduction in effective diameter) was reported as a function of NOM concentration due to steric repulsion.

Similar to the effects of IS on the effective diameter, it was expected that increasing the IS would decrease the overall EPM for both types of the MoS_2 as has been observed previously in the Chen and Elimelech (2009) study. As a baseline (lowest IS), the EPMs of MoS_2-Li and MoS_2-PL were measured in DI water and were -3.8 ± 0.1 and -1.8 ± 0.0 (10^{-8} $m^2/[V \cdot s]$), respectively. Similar IS conditions that influenced the effect on size for both types of MoS_2 were observed regarding the influence on EPM. For example, the MoS_2-Li and MoS_2-PL EPMs were not significantly affected until an IS of 31.6 and 10 mM KCl was achieved, respectively. For the MoS_2-Li, the EPM decreased from -3.8 ± 0.0 to -2.5 ± 0.4 (10^{-8} $m^2/[V \cdot s]$) across the range of 0.1–100 mM KCl. The EPM of the MoS_2-PL was also decreased from -1.7 ± 0.1 to -0.3 ± 0.3 (10^{-8} $m^2/[V \cdot s]$) across the range tested. These behaviors for both types of MoS_2 with respect to their sensitivity to IS as observed by their decrease in EPM, are in agreement with traditional Derjaguin–Landau–Verwey–Overbeek (DLVO) theory regarding the stability for colloidal particles (Verwey, 1947).

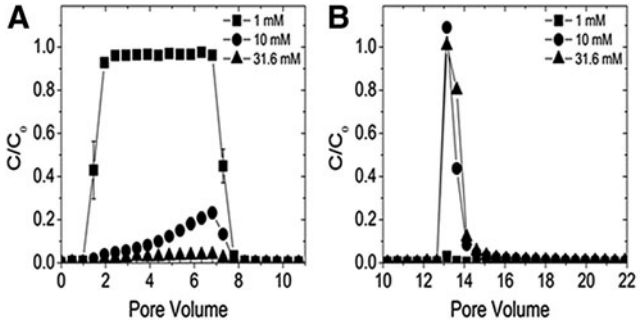

FIG. 5. Packed bed column transport results for MoS_2-PL as a function of ionic strength. **(A)** 0–10 Pore volumes: breakthrough curves as a function of IS (1–31.6 mM KCl) are an average of triplicate measurements with error bars indicating one standard deviation. **(B)** 10–22 Pore volumes: breakthrough curve after DI was injected to determine the amount of MoS_2-PL reversibly bound.

Packed bed column transport study

Column experiments were conducted with MoS_2-Li and MoS_2-PL to investigate the influence of ionic strength on the movement of MoS_2 in aquatic environments (e.g., sediment beds) across an environmentally relevant range of IS conditions (1–31.6 mM KCl at pH 5) and to determine which type of MoS_2 would be least mobile in aquatic environments. This specific range of solution chemistries was also chosen since it represents the regions where the most significant effects were observed during particle characterization (DLS and EPM) experiments. The transport results were plotted as breakthrough curves (BTCs) and are found in Figures 5 and 6. The BTCs represent the concentration of MoS_2 eluted, normalized by the injection concentration (C/C_o) as a function of PV that flowed through the column and provide a measure for the MoS_2 transport in porous media. The shapes of the BTCs also provide critical information to understand the potential deposition or retention phenomena (e.g., blocking, straining, ripening) that may be occurring during transport.

The normalized MoS_2 concentration (C/C_o) was also examined and compared at each IS for MoS_2-PL and MoS_2-Li to identify which type of MoS_2 would be least mobile in sand

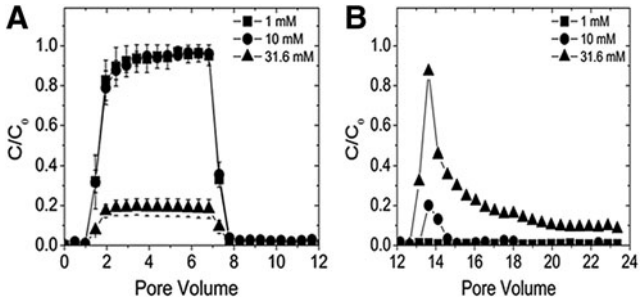

FIG. 6. Packed bed column transport results for MoS_2-Li as a function of ionic strength. **(A)** 0–12 Pore volumes: breakthrough curves as a function of IS (1–31.6 mM KCl) are an average of triplicate measurements with error bars indicating one standard deviation. **(B)** 12–24 Pore volumes: breakthrough curve after DI was injected to determine the amount of MoS_2-Li reversibly bound.

columns. In addition, the overall mass of MoS_2-PL and MoS_2-Li deposited in the column during transport was determined by integrating under the BTCs after each transport experiment and the results are shown in Table 1.

Overall, the deposition of MoS_2-Li and MoS_2-PL in the column increased for both nanomaterials as a function of IS, however, a significant effect was observed at different conditions dependent on the type of MoS_2. Specifically, no significant effect ($p > 0.05$) on MoS_2-Li transport was observed until an IS of 31.6 mM KCl was achieved, and the mass deposited was greater compared to the MoS_2-PL. For example, at 10 mM KCl the C/C_0 value was ~ 0.95 for the MoS_2-Li whereas at the same IS, the C/C_0 value for the MoS_2-PL was ~ 0.20. This difference was also observed between the two types of MoS_2 at 31.6 mM KCl where $88.7\% \pm 2.5\%$ and $96.9\% \pm 0.2\%$ of the particles were retained in the column for the MoS_2-Li and MoS_2-PL, respectively. This increase in deposition for the MoS_2-PL is interesting since these particles are roughly 19 times smaller (as measured in hydrodynamic diameter) than the MoS_2-Li counterpart. One might expect a greater retention in the column as the effective diameter of the aggregates increase due to the straining mechanism, which suggests that particles are retained and cannot pass through regions of the pore spaces due to their large size (Bradford *et al.*, 2002, 2003).

Straining can occur when the straining parameter ($d_{particle}/d_{quartz}$), which is the diameter of the particle ($d_{particle}$) divided by the diameter of the quartz collector (d_{quartz}), reaches the theoretical threshold of 0.002 (Bradford *et al.*, 2003, 2005). Straining has been used in the past during similar column transport studies to help explain removal mechanisms observed for latex particles (Porubcan and Xu, 2011), nonspherical colloids (Xu *et al.*, 2006), and other two-dimensional nanomaterials (e.g., graphene oxide) (Lanphere *et al.*, 2013). For MoS_2-PL, the effective diameter at the highest IS (31.6 mM KCl) correlated with a straining parameter (d_{MoS2}/d_{quartz}) of 0.0003, which is almost an order of magnitude below the theoretical limit of 0.002 where straining can occur. This suggests that an alternate retention mechanism is likely occurring that is responsible for the MoS_2-PL retention during transport in the porous media. The BTC observed for the MoS_2-PL at 10 mM KCl has been observed before in other transport studies and suggests that either blocking or straining is occurring. Blocking has been used in traditional colloid literature (Song and Elimelech, 1993; Liu *et al.*, 1995) to explain the deposition of colloids during transport in porous media. Blocking occurs when the particles entering the column undergo an initial rapid deposition on available collector sites, followed by a decrease in deposition rate as more deposition sites on the collectors become unavailable (Song and Elimelech, 1993; Liu *et al.*, 1995). Since the straining parameter is well below the theoretical limit, this suggests that blocking is occurring during MoS_2-PL transport in porous media. As observed by the BTC shape in Figure 5, at 10 mM KCl the MoS_2-PL undergo some massive initial deposition on the empty attachment sites located on the quartz collectors as they enter the column in the first centimeter, and then after these sites are blocked, a decrease in deposition occurs resulting in more MoS_2 being eluted from the column as a function of time. For the MoS_2-Li transport experiments, the blocking shape was not observed from the BTCs suggesting that straining may be the dominant removal mechanism during transport. This is in agreement with the straining parameter ($d_{MoS2}/d_{particle} = 0.006$) calculated for MoS_2-Li at 31.6 mM KCl. From the transport experiments it is clear that each type of MoS_2 undergo unique interactions with the quartz collectors during transport with the MoS_2-PL being the least mobile as compared with MoS_2-Li under similar conditions.

Remobilization of MoS_2

To further understand the possibility of remobilization or irreversible attachment, and to identify mechanisms by which particles are being retained (as observed from the transport experiment results described in the packed bed column transport study section) for MoS_2-Li and MoS_2-PL, DI water was injected for ~ 12 PV following a column experiment at each IS. This results in the IS strength being reduced in the column and helps to shed light on the possible mechanisms responsible for attachment, deposition, and remobilization during transport. The results from this release portion of the experiments are shown in Figures 5B and 6B for MoS_2-PL and MoS_2-Li, respectively, and have been included in Table 1. The amount of mass remobilized (collected in the effluent) after the injection of DI water was divided by the amount that

Table 1. Mass Balance Results from Column Experiments Are Also Shown, Where M_E, M_D, M_R, and M_T, Represent the Relative Mass Percent of the Mass of the MoS_2 in the Effluent, Deposited Mass Recovered from Column Dissections, Remobilized Mass After DI Injection, and the Total Mass Collected

MoS_2	*Ionic Strength (mM)*	*M_E (%)*[a]	*M_D (%)*[b]	*M_R (%)*[c]	*M_T (%)*[d]
MoS_2-PL	1	96.7 ± 1.0	19.2	18.8	115.8
	10	13.2 ± 0.2	26.3	18.0	39.4
	31.6	3.1 ± 0.2	21.7	18.8	24.8
MoS_2-Li	1	84.0 ± 7.6	28.2	3.9	112.1
	10	81.5 ± 6.5	27.8	4.8	109.2
	31.6	11.3 ± 2.5	55.9	27.4	67.2

Transport experiments were conducted using a MoS_2 concentration of 10 mg/L and a flow rate of 2 mL/min.
[a]M_E:% of mass of MoS_2 in effluent of mass injected.
[b]M_D:% of mass of MoS_2 deposited in the column and collected from the column dissection.
[c]M_R:% of MoS_2 remobilized after dispersed in (DI) injection of average retained mass from triplicate experiments.
[d]M_T:% of total mass ($M_E + M_D$) of MoS_2 in effluent (M_E) plus mass collected from column dissections (M_D).

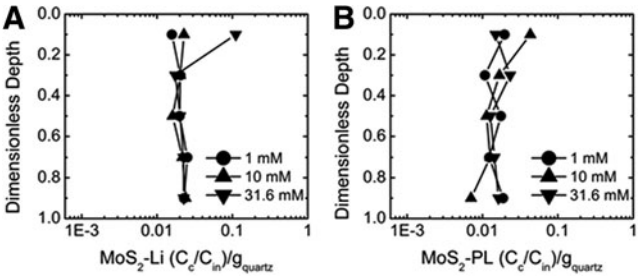

FIG. 7. Retention profiles created from the column dissections after a transport experiment in the packed bed column at 1, 10, and 31.6 mM KCl. **(A)** MoS_2-Li retention profile. **(B)** MoS_2-PL retention profile.

was retained in the column and multiplied by 100 to obtain the mass% remobilized (M_R). For the MoS_2-Li particles, the M_R increased from 4% to 27% across the IS range tested suggesting electrostatic interactions are occurring with the quartz collectors during transport and responsible for retention in the column. For the MoS_2-PL, however, the M_R remained constant (18.5% ± 0.5%) across the IS range tested suggesting a maximum remobilization regardless of IS. This difference in remobilization phenomena between the two types of MoS_2 suggests that the PF-87 pluronic surfactant on the MoS_2-PL is interacting with the quartz collectors, resulting in a strong bond and a limited M_R. The interactions between the PEO functional groups present on the MoS_2-PL surface and the Si function groups on the quartz collector are likely forming strong intermolecular bonds and resulting in irreversible attachment. This irreversible attachment was not observed in other two-dimensional planar particles (i.e., graphene oxide) that exhibited ~100% remobilization once DI water was injected during the release portion of a column experiment (Feriancikova and Xu, 2012; Lanphere *et al.*, 2013). The release experiments highlight the different behaviors for MoS_2 during transport in sand columns; with MoS_2-PL being the least sensitive to change in IS and less mobile compared with MoS_2-Li when the remobilization (M_R) parameter was considered at similar conditions.

Spatial distribution of MoS_2 in the column

To provide additional insight into the unique differences observed in the transport and release experimental results between the two types of MoS_2; the distribution of MoS_2 deposited at each centimeter during transport was quantified using previously described methods (Lanphere *et al.*, 2013) and is reported in Figure 7. Overall, the majority of MoS_2-Li was equally distributed throughout each centimeter of the column for at the lower IS (1–10 M KCl) tested. However, once 31.6 mM KCl was achieved, a sharp increase (approximately seven times greater compared with 1 mM KCl condition) in MoS_2-Li mass deposited in the top centimeter of the column was observed as seen in Figure 7B. This increase in deposition in the top centimeter of the column correlates well with the effective diameter (~1512 nm at 31.6 mM KCl) characterized in the DLS experiments, which results in a straining parameter (d_{MoS2}/d_{quartz}) of 0.006, suggesting that straining is the removal mechanism occurring at this condition. However, for the MoS_2-PL there was no significant difference ($p > 0.05$) in spatial distribution as a function of IS. The retention profiles were very similar across the range of IS tested (1–31.6 mM KCl). The equal spatial distribution of MoS_2-PL in the retention profiles suggest that they are being irreversibly attached to the quartz collectors and is in agreement to the trend observed during the release portion of the column experiments.

DLVO theory

DLVO theory was used to identify whether the trends observed during the column transport experiments were due to MoS_2–quartz interactions (blocking) or MoS_2–MoS_2 interactions (straining). Calculations were performed using traditional DLVO theory (Verwey, 1947; Derjaguin and Landau, 1993) to simulate MoS_2–quartz interactions, assuming a constant potential and sphere-plate geometry (Hogg *et al.*, 1966) and can be seen in Tables 2 and 3. A Hamaker constant of 6.26×10^{-21} J was used for the MoS_2_water–quartz systems (Feriancikova and Xu, 2012), and the EPM measurements for the MoS_2 nanomaterials were converted to zeta potential values using the Smoluchowski equation (Elimelech, 1995). The MoS_2–Li interaction energy profile at 31.6 mM KCl suggest that a secondary minimum (−5.7 kT) exists at 10 nm. This secondary minimum at 31.6 mM KCl may help explain why there was twice as much deposition in the column compared with the 1 mM KCl condition. For the MoS_2-PL DLVO profiles, there was only a small energy barrier (1.9 kT) at 10 mM KCl and no energy barrier at 31.6 mM KCl observed. This absence of an energy barrier for MoS_2_quartz surfaces at 31.6 mM KCl likely contributed to the fraction (26%) of irreversibly bound particles retained in the column following the release portion of the transport experiments. This is also in agreement with what was observed in the retention profiles where 78% of the MoS_2-PL particles remained on the quartz collectors even

TABLE 2. RESULTS FROM CALCULATIONS BASED UPON DLVO AND THE SPHERE-PLATE ASSUMPTION FOR MoS_2-LI NANOPARTICLES AND QUARTZ COLLECTORS

IS (mM KCl)	*Zeta potential of MoS_2 (mV)*	*Zeta potential of quartz (mV)*	*1° energy barrier (kT)*	*1°energy barrier separation distance (nm)*	*2°min depth (kT)*	*2°min separation distance (nm)*	*Diameter*[a] *(nm)*	*EPM*[b] *(10^{-8} m^2 [V·s])*
1	−52.4 ± 3.2	−28.6 ± 2.0	260.4	2.5	−0.018	109.5	338.5 ± 9.6	−4.1 ± 0.3
10	−50.7 ± 1.7	−13.6 ± 0.5	52.8	2.5	−0.32	24	342.2 ± 4.9	−4.0 ± 0.1
31.6	−41.7 ± 1.0	−11.3 ± 1.4	97.6	2.0	−5.7	10	1512.5 ± 210.8	−3.3 ± 0.1

[a]Average hydrodynamic diameter values for MoS_2-Li were experimentally recorded and were used in the Derjaguin-Landau-Verwey-Overbeek (DLVO) calculations.
[b]Electrophoretic mobility (EPM) values for MoS_2-Li were used to calculate zeta potentials through the Smoluchowski equation (Elimelech, 1995).

TABLE 3. RESULTS FROM CALCULATIONS BASED UPON DLVO AND THE SPHERE-PLATE ASSUMPTION FOR MoS_2-PL NANOPARTICLES AND QUARTZ COLLECTORS

IS (mM KCl)	*Zeta potential of MoS_2 (mV)*	*Zeta potential of quartz (mV)*	*1° energy barrier (kT)*	*1° energy barrier separation distance (nm)*	*2° min depth (kT)*	*2° min separation distance (nm)*	*Diameter* (nm)*	*EPM** (10^{-8} m^2 V^{-1} s^{-1})*
10^{-3}	−21.0 ± 1.8	−28.6 ± 2.0	24.1	2.0	−0.005	95.5	75.4 ± 1.0	−1.6 ± 0.1
10^{-2}	−11.4 ± 1.0	−13.6 ± 0.5	1.9	2.5	−0.13	16	83.4 ± 2.8	−0.9 ± 0.1
$10^{-1.5}$	−5.3 ± 1.1	−11.3 ± 1.4	None (−2.6)	2.0	None	N/A	79.7 ± 2.4	−0.4 ± 0.1

*Average hydrodynamic diameter values were experimentally recorded and were used in the DLVO calculations.
**EPM values for MoS_2-Li were used to calculate zeta potentials via the Smoluchowski equation (Elimelech 1995).

after being chemically (reduction in IS) and physically (vortexed) perturbed.

To further explain the transport results observed in this study, MoS_2–MoS_2 interactions were considered and additional DLVO interaction energy profiles were created. A secondary energy minimum (−1.8 kT at 15 nm) was observed for the MoS_2-Li at 31.6 mM KCl, which correlates with the straining parameter (0.006) that was calculated and the seven-fold increase (compared to the 1 mM KCl condition) in mass deposited in the first centimeter as observed in the retention profiles (Fig. 7A). A similar trend was observed in previous reports for another two-dimensional nanomaterial (graphene oxide) (Feriancikova and Xu, 2012), and it was reported that the existence of a secondary minimum contributed to the removal of graphene oxide particles during transport through reversible chemical (electrostatic) interactions. For the MoS_2-PL a secondary minimum was not observed when MoS_2–MoS_2 interactions were considered.

Overall, DLVO interaction energy profiles helped provide additional information regarding the individual removal mechanisms for each type of MoS_2 during transport in sand columns. Specifically, the application of DLVO supports the claim that straining is the dominant mechanism for retention in porous media occurring at higher IS for MoS_2-Li due to secondary energy minimums present, which results in aggregation of the MoS_2-MoS_2 particles. It is also likely that the smaller MoS_2-PL nanomaterials are experiencing deeper primary minimum interactions compared to the MoS_2-Li since they are smaller in size and is in agreement with the trends observed in previous studies (Bradford and Torkzaban, 2012, 2013). This difference in primary interactions between MoS_2-PL and MoS_2-Li may help explain why greater amounts of MoS_2-PL (86.8% ± 0.2%) were retained in the column at similar IS (10 mM KCl) compared with MoS_2-Li (18.5% ± 6.5%) even though the particles were smaller. Furthermore, the application of DLVO helps support the mechanistic explanation that MoS_2-PL likely undergoes irreversible attachment to the quartz collectors due to the absence of (or minimal) energy barriers present during interactions with quartz collectors. These irreversible interactions contributed to the decreasing rate of MoS_2-PL retention over time as observed by the blocking phenomena seen in the BTC shape during transport experiments. This is in agreement with the trends observed in the limited remobilization (M_R = 18.6% ± 0.5%) during release experiments and the equal spatial distribution of MoS_2-PL throughout the column in the retention profiles.

SEM images of quartz sand and MoS_2

SEM images were taken to better understand the role of physical interactions between the MoS_2 and sand grains as a

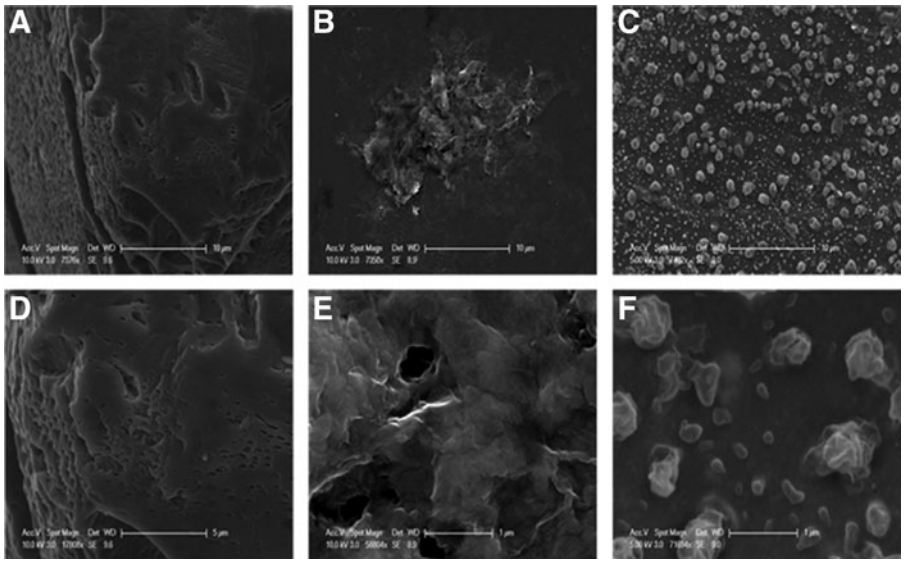

FIG. 8. Scanning Electron Microscopy (SEM) images taken at different magnifications for quartz collectors and MoS_2-Li and MoS_2-PL particles used in the packed bed column experiments. **(A, D)** Quartz collector at 10 and 5 μm. **(B, E)** MoS_2-Li at 10 and 1 μm. **(C, F)** MoS_2-PL at 10 and 1 μms.

function of their different surface morphologies and to identify any potential physical removal mechanisms during transport. The SEM images shown in Figure 8 suggest that the physical geometry (two-dimensional planar flakes) of the MoS_2 likely plays an important role during transport through porous media. It is likely that the planar MoS_2 particles get wedged or removed during transport since their shape and size allow them to interact with the rough surface of the quartz sand. As seen in Figure 8A and D, the surface of the quartz collectors is very heterogeneous with craters and pits ranging from 1 to 2 μm in diameter. In addition, the MoS_2-Li (Fig. 8B, E) and MoS_2-PL (Fig. 8C, F) SEM images taken highlight the unique two dimension planar sheet-like structure of the MoS_2 particles. As a result of this geometry, van der Waals forces would have a greater influence since the large surface area of the MoS_2 is able to interact with the surface of the quartz surfaces. This is consistent with the DLVO calculations that revealed an absence in energy barrier for MoS_2-PL and quartz surfaces, and may explain why there was greater MoS_2-PL retention in the column during transport compared with MoS_2-Li even though the size (as measured in DLS experiments) was $\sim$19 times smaller at 31.6 mM KCl. Furthermore, it is likely that both types of MoS_2 are experiencing some wedging or straining as they transport through the column and interact with the rough surfaces on the quartz collectors. This assumption is consistent with others who have reported that wedging and straining are the mechanistic basis for colloid retention during transport in porous media (Bradford *et al.*, 2002, 2005; Johnson *et al.*, 2007).

Summary and Conclusions

This study highlights the different fate and transport mechanisms for two common types of MoS_2 in aquatic environments. A comprehensive study was performed to identify the unique behaviors of MoS_2-Li and MoS_2-PL in aqueous environments to better understand which type of MoS_2 would be least mobile and likely be exposed to various aquatic species (e.g., benthic feeders) in sediment beds. Traditional methods used to synthesize MoS_2-Li may result in increased transport in sediment beds and aquatic systems under environmentally relevant conditions (1–10 mM KCl). However, at higher IS ($\geq$31.6 mM KCl), MoS_2-Li will become less stable and aggregate to sizes greater than 1.5 μm. Under these conditions, MoS_2-Li will likely be removed through straining and as a result of secondary minimum interactions in sediment beds may potentially bio-accumulate in benthic organisms. Conversely, the MoS_2-PL will tend to transport farther in aqueous systems due to its stable characteristics at environmental conditions (pH 5–9). If MoS_2-PL comes into contact with quartz media in the subsurface, it will have a higher affinity to be deposited and attach as a result of the reduced energy barrier between MoS_2-PL + quartz surfaces as observed from transport experiments and column dissections in this study. Additionally, as observed in the SEM images, the two-dimensional planar geometry of both types of MoS_2 nanomaterials will likely contribute to the physical removal of individual flakes during transport in porous media as a result of being wedged into heterogeneous pits present on quartz surfaces. As a result of the chemical and physical mechanisms contributing to the removal during transport in porous media, this study confirms that MoS_2-PL will be the least mobile type of MoS_2 in aquatic environments compared to MoS_2-Li.

Acknowledgments

This article is based upon the work supported by the National Science Foundation Graduate Research Fellowship under Grant No. (DGE-0813967) and the University of California Center for the Environmental Implications of Nanotechnology (UC-CEIN) (National Science Foundation and Environmental Protection Agency under Cooperative Agreement # DBI-1266377). Any opinion, findings, and conclusions or recommendations expressed in this article are those of the authors and do not necessarily reflect the views of the National Science Foundation or the Environmental Protection Agency. This work has not been subjected to EPA review and no official endorsement should be inferred. Finally, the authors are thankful for the help from undergraduate research assistant Corey Luth (also funded by UC CEIN) and Dr. Nichola Kinsinger for her help in obtaining the SEM images used in this study.

Author Disclosure Statement

No competing financial interest exists.

References

Bradford, S.A., Simunek, J., Bettahar, M., Tadassa, Y.F., van Genuchten, M.T., and Yates, S.R. (2005). Straining of colloids at textural interfaces. *Water Resour. Res.* 41, 10.

Bradford, S.A., Simunek, J., Bettahar, M., Van Genuchten, M.T., and Yates, S.R. (2003). Modeling colloid attachment, straining, and exclusion in saturated porous media. *Environ. Sci. Technol.* 37, 2242.

Bradford, S.A., and Torkzaban, S. (2012). Colloid adhesive parameters for chemically heterogeneous porous media. *Langmuir.* 28, 13643.

Bradford, S.A., and Torkzaban, S. (2013). Colloid interaction energies for physically and chemically heterogeneous porous media. *Langmuir.* 29, 3668.

Bradford, S.A., Yates, S.R., Bettahar, M., and Simunek, J. (2002). Physical factors affecting the transport and fate of colloids in saturated porous media. *Water Resour. Res.* 38.

Chen, K.L., and Elimelech, M. (2006). Aggregation and deposition kinetics of fullerene (C-60) nanoparticles. *Langmuir.* 22, 10994.

Chen, K.L., and Elimelech, M. (2009). Relating colloidal stability of fullerene (C-60) nanoparticles to nanoparticle charge and electrokinetic properties. *Environ. Sci. Technol.* 43, 7270.

Chowdhury, I., Cwiertny, D.M., and Walker, S.L. (2012a). Combined factors influencing the aggregation and deposition of nano-TiO2 in the presence of humic acid and bacteria. *Environ. Sci. Technol.* 46, 6968.

Chowdhury, I., Duch, M.C., Gits, C.C., Hersam, M.C., and Walker, S.L. (2012b). Impact of synthesis methods on the transport of single walled carbon nanotubes in the aquatic environment. *Environ. Sci. Technol.* 46, 11752.

Chowdhury, I., Duch, M.C., Mansukhani, N.D., Hersam, M.C., and Bouchard, D. (2013). Colloidal properties and stability of graphene oxide nanomaterials in the aquatic environment. *Environ. Sci. Technol.* 47, 6288.

Chowdhury, I., Hong, Y., Honda, R.J., and Walker, S.L. (2011). Mechanisms of TiO2 nanoparticle transport in porous media:

Role of solution chemistry, nanoparticle concentration, and flowrate. *J. Colloid. Interf. Sci.* 360, 548.

Compton, O.C., and Nguyen, S.T. (2010). Graphene oxide, highly reduced graphene oxide, and graphene: Versatile building blocks for carbon-based materials. *Small.* 6, 711.

Conway, J.R., Hanna, S.K., Lenihan, H.S., and Keller, A.A. (2014). Effects and implications of trophic transfer and accumulation of CeO2 nanoparticles in a marine mussel. *Environ. Sci. Technol.* 48, 1517.

Cooper, R.C., Lee, C., Marianetti, C.A., Wei, X., Hone, J., and Kysar, J.W. (2013). Nonlinear elastic behavior of two-dimensional molybdenum disulfide. *Phys. Rev. B.* 87, 035423.

Crittenden, J.C., Trussell, R.R., Hand, D.W., Howe, K.J., and Tchobanoglous, G. (2012). Physical and chemical quality of water. *In MWH's Water Treatment: Principles and Design*, Third Edition. Hoboken, NJ: John Wiley & Sons, Inc., pp. 17–71.

Derjaguin, B., and Landau, L. (1993). Theory of the stability of strongly charged lyophobic sols and of the adhesion of strongly charged-particles in solutions of electrolytes. *Prog. Surf. Sci.* 43, 30.

Duch, M.C., Budinger, G.R.S., Liang, Y.T., Soberanes, S., Urich, D., Chiarella, S.E., Campochiaro, L.A., Gonzalez, A., Chandel, N.S., Hersam, M.C., and Mutlu, G.M. (2011). Minimizing oxidation and stable nanoscale dispersion improves the biocompatibility of graphene in the lung. *Nano Lett.* 11, 5201.

Elimelech, M., and Omelia, C.R. (1990). Effect of particle-size on collision efficiency in the deposition of brownian particles with electrostatic energy barriers. *Langmuir.* 6, 1153.

Elimelech, M., Gregory, J., Jia, X., and Williams, R.A. (1995). *Particle Deposition and Aggregation: Measurements, Modeling, and Simulation.* Oxford, UK: Butterworth-Heinemann.

Feriancikova, L., and Xu, S.P. (2012). Deposition and remobilization of graphene oxide within saturated sand packs. *J. Hazard. Mater.* 235, 194.

Gong, Y., Liu, Z., Lupini, A.R., Shi, G., Lin, J., Najmaei, S., Lin, Z., Elías, A.L., Berkdemir, A., You, G., Terrones, H., Terrones, M., Vajtai, R., Pantelides, S.T., Pennycook, S.J., Lou, J., Zhou, W., and Ajayan, P.M. (2013). Band gap engineering and layer-by-layer mapping of selenium-doped molybdenum disulfide. *Nano Lett.* 14, 442.

Hemond, H.F., Fechner-Levy, E.J. (2009). *Chemical Fate and Transport in the Environment*. San Diego: Academic Press.

Hogg, R., Healy, T.W., and Fuersten.Dw. (1966). Mutual Coagulation of Colloidal Dispersions. *Trans. Faraday Soc.* 62, 1638.

Johnson, W.P., Li, X., and Yal, G. (2007). Colloid retention in porous media: mechanistic confirmation of wedging and retention in zones of flow stagnation. *Environ. Sci. Technol.* 41, 1279.

Keller, A.A., McFerran, S., Lazareva, A., and Suh, S. (2013). Global life cycle releases of engineered nanomaterials. *J. Nanopart. Res.* 15.

Keller, A.A., Wang, H., Zhou, D., Lenihan, H.S., Cherr, G., Cardinale, B.J., Miller, R., and Ji, Z. (2010a). Stability and aggregation of metal oxide nanoparticles in natural aqueous matrices. *Environ. Sci. Technol.* 44, 1962.

Keller, A.A., Wang, H.T., Zhou, D.X., Lenihan, H.S., Cherr, G., Cardinale, B.J., Miller, R., and Ji, Z.X. (2010b). Stability and aggregation of metal oxide nanoparticles in natural aqueous matrices. *Environ. Sci. Technol.* 44, 1962.

Khare, H.S., and Burris, D.L. (2014). Surface and subsurface contributions of oxidation and moisture to room temperature friction of molybdenum disulfide. *Tribol. Lett.* 53, 329.

Lanphere, J.D., Luth, C.J., and Walker, S.L. (2013). Effects of solution chemistry on the transport of graphene oxide in saturated porous media. *Environ. Sci. Technol.* 47, 4255.

Lauritsen, J.V., Kibsgaard, J., Helveg, S., Topsoe, H., Clausen, B.S., Laegsgaard, E., and Besenbacher, F. (2007). Size-dependent structure of MoS2 nanocrystals. *Nat. Nanotechnol.* 2, 53.

Liu, D., Johnson, P.R., and Elimelech, M. (1995). Colloid deposition dynamics in flow-through porous media: Role of electrolyte concentration. *Environ. Sci. Technol.* 29, 2963.

Liu, K., Feng, J., Kis, A., and Radenovic, A. (2014). Atomically thin molybdenum disulfide nanopores with high sensitivity for DNA translocation. *Acs. Nano.* 8, 2504.

Lopez-Sanchez, O., Lembke, D., Kayci, M., Radenovic, A., and Kis, A. (2013). Ultrasensitive photodetectors based on monolayer MoS2. *Nat. Nanotechnol.* 8, 497.

Lotya, M., Hernandez, Y., King, P.J., Smith, R.J., Nicolosi, V., Karlsson, L.S., Blighe, F.M., De, S., Wang, Z.M., McGovern, I.T., Duesberg, G.S., and Coleman, J.N. (2009). Liquid phase production of graphene by exfoliation of graphite in surfactant/water solutions. *J. Am. Chem. Soc.* 131, 3611.

Mak, K.F., Lee, C., Hone, J., Shan, J., and Heinz, T.F. (2010). Atomically Thin MoS_2: A new direct-gap semiconductor. *Phys. Rev. Lett.* 105, 136805.

Mohd Omar, F., Abdul Aziz, H., and Stoll, S. (2014). Aggregation and disaggregation of ZnO nanoparticles: Influence of pH and adsorption of Suwannee River humic acid. *Sci. Total Environ.* 468–469, 195.

Najmaei, S., Zou, X., Er, D., Li, J., Jin, Z., Gao, W., Zhang, Q., Park, S., Ge, L., Lei, S., Kono, J., Shenoy, V.B., Yakobson, B.I., George, A., Ajayan, P.M., and Lou, J. (2014). Tailoring the physical properties of molybdenum disulfide monolayers by control of interfacial chemistry. *Nano. Lett.* 14, 1354.

Petosa, A.R., Brennan, S.J., Rajput, F., and Tufenkji, N. (2012). Transport of two metal oxide nanoparticles in saturated granular porous media: Role of water chemistry and particle coating. *Water Res.* 46, 1273.

Petosa, A.R., Jaisi, D.P., Quevedo, I.R., Elimelech, M., and Tufenkji, N. (2010). Aggregation and deposition of engineered nanomaterials in aquatic environments: Role of physicochemical interactions. *Environ. Sci. Technol.* 44, 6532.

Porubcan, A.A., and Xu, S. (2011). Colloid straining within saturated heterogeneous porous media. *Water Res.* 45, 1796.

Seo, J.-W.T., Green, A.A., Antaris, A.L., and Hersam, M.C. (2011). High-Concentration aqueous dispersions of graphene using nonionic, biocompatible block copolymers. *J. Phys. Chem. Lett.* 2, 1004.

Silbernagel, B.G. (1975). Lithium intercalation complexes of layered transition-metal dichalcogenides—NMR survey of physical-properties. *Solid State Commun.* 17, 361.

Song, L., and Elimelech, M. (1993). Dynamics of colloid deposition in porous media: Modeling the role of retained particles. *Colloids Surf. A Physicochem. Eng. Aspects.* 73, 49.

Stephenson, T., Li, Z., Olsen, B., and Mitlin, D. (2014). Lithium ion battery applications of molybdenum disulfide (MoS2) nanocomposites. *Energ. Environ. Sci.* 7, 209.

Tufenkji, N., and Elimelech, M. (2004). Deviation from the classical colloid filtration theory in the presence of repulsive DLVO interactions. *Langmuir.* 20, 10818.

Vaisman, L., Wagner, H.D., and Marom, G. (2006). The role of surfactants in dispersion of carbon nanotubes. *Adv. Colloid Interfac.* 128, 37.

Verwey, E.J.W. (1947). Theory of the stability of lyophobic colloids. *J. Phys. Colloid Chem.* 51, 631.

Wang, H., Qi, J., Keller, A.A., Zhu, M., and Li, F. (2014). Effects of pH, ionic strength and humic acid on the removal of TiO2 nanoparticles from aqueous phase by coagulation. *Colloids Surf. A. Physicochem. Eng. Aspects.* 450, 161.

Wang, Q.H., Kalantar-Zadeh, K., Kis, A., Coleman, J.N., and Strano, M.S. (2012a). Electronics and optoelectronics of two-dimensional transition metal dichalcogenides. *Nat. Nanotechnol.* 7, 699.

Wang, Q.H., Kalantar-Zadeh, K., Kis, A., Coleman. J.N., Strano, M.S. (2012b). Graphene is not alone. *Nat. Nanotechnol.* 7, 683.

Ward, G.M. (1978). Molybdenum toxicity and hypocuprosis in ruminants—review. *J. Anim. Sci.* 46, 1078.

Wiesner, M.R., and Lecoanet, H. (2004). Aggregation and deposition characteristics of fullerene nanoparticles in aqueous systems. *Abstr. Pap. Am. Chem. S.* 228, U606.

Winchester, A., Ghosh, S., Feng, S., Elias, A.L., Mallouk, T., Terrones, M., and Talapatra, S. (2014). Electrochemical characterization of liquid phase exfoliated two-dimensional layers of molybdenum disulfide. *Acs. Appl. Mater. Inter.* 6, 2125.

Wu, H., Yang, R., Song, B., Han, Q., Li, J., Zhang, Y., Fang, Y., Tenne, R., and Wang, C. (2011). Biocompatible inorganic fullerene-like molybdenum disulfide nanoparticles produced by pulsed laser ablation in water. *Acs. Nano.* 5, 1276.

Xie, B., Xu, Z., Guo, W., and Li, Q. (2008). Impact of natural organic matter on the physicochemical properties of aqueous C60 nanoparticles. *Environ. Sci Technol.* 42, 2853.

Xu, S., Gao, B., and Saiers, J.E. (2006). Straining of colloidal particles in saturated porous media. *Water Resour. Res.* 42, W12S16.

Yin, T., Walker, H.W., Chen, D., and Yang, Q. (2014). Influence of pH and ionic strength on the deposition of silver nanoparticles on microfiltration membranes. *J. Membr. Sci.* 449, 9.

Zhang, H., Lu, S.B., Zheng, J., Du, J., Wen, S.C., Tang, D.Y., and Loh, K.P. (2014). Molybdenum disulfide (MoS2) as a broadband saturable absorber for ultra-fast photonics. *Opt. Express.* 22, 7249.

Zhou, W., Zou, X., Najmaei, S., Liu, Z., Shi, Y., Kong, J., Lou, J., Ajayan, P.M., Yakobson, B.I., and Idrobo, J.-C. (2013). Intrinsic structural defects in monolayer molybdenum disulfide. *Nano Lett.* 13, 2615.